Synthesis and Characterization of 4-Vinylimidazolium/Styrene-Cografted Anion-Conducting Electrolyte Membranes

Takashi Hamada,[†,] Kimio Yoshimura, Kota Takeuchi, Shun Watanabe, Yue Zhao, Akihiro Hiroki, Tokio Hagiwara, Hideyuki Shishitani, Susumu Yamaguchi, Hirohisa Tanaka,[††] Aurel Radulescu, Kenji Ohwada, and Yasunari Maekawa**

Dr. Takashi Hamada, Dr. Kimio Yoshimura, Dr. Yue Zhao, Dr. Akihiro Hiroki, and Dr. Yasunari Maekawa
Department of Advanced Functional Materials Research, Takasaki Advanced Radiation Research Institute, Quantum Beam Science Research Directorate, National Institutes for Quantum and Radiological Science and Technology (QST), 1233 Watanuki, Takasaki, Gunma 370-1292, Japan
E-mail: maekawa.yasunari@qst.go.jp

[†]Present address:
Lecturer T. Hamada
Graduate School of Advanced Science and Engineering, Hiroshima University, 1-4-1 Kagamiyama, Higashi-Hiroshima, Hiroshima 739-8527, Japan
E-mail: hama@hiroshima-u.ac.jp

Kota Takeuchi, and Visiting Prof. Y Maekawa
Graduate School of Science and Technology, Gunma University, 1-5-1 Tenjin-cho, Kiryu, Gunma 376-8515, Japan

Shun Watanabe, and Prof. Hagiwara
Graduate School of Engineering, Saitama Institute of Technology, 1690 Fusaiji, Fukaya, Saitama 369-0293, Japan

Hideyuki Shishitani, Dr. Susumu Yamaguchi, and Dr. Hirohisa Tanaka
Daihatsu Motor Co., Ltd., 3000 Ohaza Yamanoue, Ryuo Gamo, Shiga 520-2593, Japan

[††]Present address:
Prof. H. Tanaka
School of Science and Technology, Kwansei Gakuin University, 2-1 Gakuen, Sanda, Hyogo 669-1337, Japan

Dr. Aurel Radulescu
Forschungszentrum Jülich GmbH, Jülich Centre for Neutron Science@MLZ, Lichtenbergstraße 1, D-85747 Garching, Germany

Dr. Kenji Ohwada
Synchrotron Radiation Research Center, Quantum Beam Science Research Directorate, National Institutes for Quantum and Radiological Science and Technology (QST), 1-1-1 Kouto, Sayo, Hyogo 679-5148, Japan

Keywords: anion-conducting electrolyte membrane, radiation-induced graft polymerization, poly(ethylene-co-tetrafluoroethylene), imidazole, alkaline durability

Abstract

The β-hydrogen-free imidazole monomer, 2-methyl-*N*-methyl-4(5)-vinylimidazole (2M4VIm), was synthesized to prepare anion exchange membranes (AEMs). The radiation-induced graft polymerization of 2M4VIm and styrene was performed in poly(ethylene-co-tetrafluoroethylene) (ETFE), followed by *N*-alkylation and ion exchange reactions to prepare 4-vinylimidazolium-containing AEM (2M4VIm/St-AEM). AEMs that have a 6/4 2M4VIm/St molar ratio and 1.7 mmol/g ion exchange capacity (IEC) resulted in 75 mS/cm conductivity and 60% water uptake at room temperature in water, demonstrating enhanced values compared to previously reported 2-methyl-*N*-vinylimidazolium-containing AEMs (2MNVIm/St-AEM) that have a similar comonomer ratio and IEC. The small-angle neutron scattering measurements of dry and swollen 2M4VIm/St-AEM revealed hydrophilic/hydrophobic two-phase separation, as observed for 2MNVIm/St-AEM with a similar Im/St composition. 2M4VIm/St-AEMs exhibited higher alkaline stability in 1 M KOH at 80 °C at an early stage owing to the suppression of imidazolium β-elimination but lower long-term stability than that of 2MNVIm/St-AEM due to the ring-opening reaction of the imidazolium group due to its outward orientation from the graft main chain.

1. Introduction

Proton exchange membrane (PEM) fuel cells (PEMFCs) promise to reduce fossil fuel consumption and CO_2 emissions, offering an environmentally friendly solution compared to conventional approaches.[1] For the next-generation power source, PEMFCs have been applied to fuel cell vehicles and stationary cogeneration systems.[2] Due to its high conductivity and chemical and mechanical stability, Nafion has been currently used as a typical PEM.[3] PEMs usually comprise sulfonic acids, which exhibit high acidity and provide fuel cells with excellent conducting properties. Usually, PEMFCs are composed of PEMs and noble metal electrodes.

Because highly acidic sulfonic acid dissolves nonprecious metals, PEMFCs require precious metals as electrodes, making their use highly costly.

In the recent years, anion exchange membrane (AEM)-based fuel cells (AEMFCs) have received attention because, unlike PEMs, AEMs function in alkaline conditions that do not dissolve nonprecious metals,[4] making AEMs a cost-effective alternative to the noble metal dependence of PEMs.[5] However, the practical applications of AEMFCs are still challenging because their conductivity and long-term durability are insufficient for practical applications compared with those of PEMFCs. In particular, the long-term chemical stability of AEMs under alkaline conditions at high temperatures must be realized to employ AEMFCs in practical applications. So far, both base polymers and ionic groups have been studied to improve the chemical stability of AEMs. Although AEMs based on poly(arylene ether)s,[6] poly(phenylene oxide),[7] and poly(ether ether ketone)[8] as base polymers and the quaternary alkylammonium group[9] and the imidazolium group[10] as ionic groups have been proposed, these AEMs fall short of meeting the required stability and properties for practical applications.

Graft-type AEMs[11] prepared by radiation-induced graft polymerization followed by quaternization and ion exchange reactions are one of the promising candidates for improving the chemical stability of AEMFCs because of the introduction of functional grafted polymers directly bonded to mechanically tough base polymers. Since poly(ethylene-co-tetrafluoroethylene) (ETFE) possesses excellent mechanical strength and chemical stability, we have developed graft-type AEMs based on ETFE, as shown in **Scheme 1**.[12] The structure–property relationship by small-angle X-ray scattering and small-angle neutron scattering (SANS) methods have also been studied for the graft-type AEMs.[13]

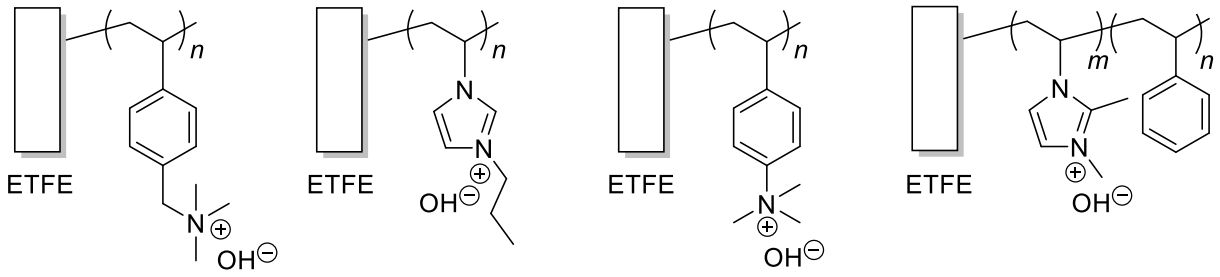

ETFE = $\left(CH_2CH_2-CF_2CF_2\right)_n$

Scheme 1. Structures of TMA-AEM, Im-AEM, An-AEM, and 2MNV/St-AEM.

The graft-type AEM that has highly basic tetramethylammonium hydroxide, namely, poly(vinylbenzyltrimethylammonium hydroxide)-grafted ETFE (TMA-AEM) made the ETFE-based polymers severely damaged in alkaline conditions at high temperatures.[12a,12d] The physical decomposition that causes film fragmentation was observed in an alkaline solution at a relatively high temperature due to the self-base-catalyzed decomposition of ETFE chains in highly basic tetramethylammonium hydroxide. For reducing the self-base-catalyzed decomposition of AEMs, we replaced the alkylammonium group with the phenylammonium group (poly(trimethylphenylammonium hydroxide)-grafted ETFE (An-AEM))[12d] and the imidazolium group (poly(1-vinyl-3-propylimidazolium hydroxide)-grafted ETFE (Im-AEM)).[12b] With a similar ion exchange capacity (IEC), An-AEM exhibited lower conductivity and water uptake than TMA-AEM, and the membrane shape of An-AEM was maintained in alkaline solutions at high temperatures. Unfortunately, the methanol was eliminated from the quaternized trimethylphenyl cation by the nucleophilic attack of hydroxide ions in alkaline conditions at high temperatures. In contrast, imidazolium-type AEMs exhibited lower water uptake than the corresponding AEM that contains trimethylammonium hydroxide because of the lower basicity of imidazolium hydroxide as an Arrhenius base.[14] Furthermore, AEMs containing weak-base imidazolium groups induce less damage to the polymer backbone due to

self-base-catalyzed degradation. However, Im-AEM prepared from commercially available *N*-vinylimidazole as a graft monomer was subjected to severe β-elimination and ring-opening hydrolysis of imidazolium groups.[12b] Thus, we used styrene as a comonomer in the radiation-induced graft polymerization of *N*-vinylimidazole into ETFE. We found that the hydrophobic styrene in the graft chain suppressed the β-elimination of the imidazolium group.[12b] Then, to prevent the ring-opening hydrolysis, we modified the imidazolium-type AEMs by radiation-induced graft polymerization of 2-methyl-*N*-vinylimidazole (2MNVIm), which has a methyl-protecting group at the C2 position of the imidazolium ring, and cografting with hydrophobic styrene into ETFE.[12e] The obtained poly(1,2-dimethyl-*N*-vinylimidazolium hydroxide-co-styrene)-grafted ETFE (2MNVIm/St-AEM) exhibited lower damage in the ETFE base film and higher alkaline stability than TMA-AEM and Im-AEM due to low basicity and a methyl group at the C2 position of the imidazolium group.[12e] Accordingly, 2MNVIm/St-AEM can offer enhanced electrical and mechanical properties. However, the β-elimination of the imidazole group in the AEM was observed at a very early stage of immersion in 1 M KOH at 80 °C; in other words, the introduction of hydrophobic styrene was insufficient to prevent β-elimination. Thus, further improvement is desired to obtain a graft-type AEM with high alkaline durability.

In this paper, we synthesized a new imidazole monomer, 2-methyl-*N*-methyl-4(5)-vinylimidazole (2M4VIm), and 2M4VIm and styrene-cografted AEM by radiation-induced graft polymerization, *N*-alkylation, and ion exchange reaction to fully prevent β-elimination reaction and introduce methyl groups at the C1 and C2 positions to prevent hydroxide attack leading to ring-opening hydrolysis.[12c] To enable this synthesis, our strategy is as follows: (1) 2M4VIm has the methyl group at the C1 and C2 positions to prevent the ring-opening reaction by the hydroxide ion, (2) the vinyl group is located at the C4 position of the imidazolium group to prevent the β-elimination of the imidazolium group from the graft chain (the β-hydrogen is eliminated from the imidazole structure), and (3) the hydrophobic styrene was cografted with

2M4VIm to prevent the hydrolysis of the imidazolium group. The conductivity, water uptake, and mechanical property of the AEMs and their alkaline stability in 1 M KOH at 80 °C were investigated and compared with that of 2MNVIm/St-AEM. Finally, to understand the effects of the AEM structure on the electrolyte properties and durability, we discussed the hierarchical structure of the graft-type AEM having the β-hydrogen-free imidazole using the SANS method.

2. Experimental Section/Methods

2.1. Materials

ETFE films with a thickness of 25 μm and a crystallinity of 35% was purchased from DuPont and used as a base film. Urocanic acid was purchased from Sigma-Aldrich and used as received. The sodium hydroxide and 2.6 M *n*-butyllithium (*n*-BuLi) in *n*-hexane were purchased from Kanto Chemical Co., Ltd and used as received. Potassium carbonate (K_2CO_3) was purchased from Kishida Chemical Co., Ltd. and dried before use. Styrene, iodomethane, hexane (super dehydrated), *N,N*-dimethylformamide (DMF, super dehydrated), tetrahydrofurane (THF, super dehydrated, stabilizer free), and dichloromethane were purchased from FUJIFILM Wako Pure Chemical Co., Ltd. and used without further purification. The water used in the experiments was purified using a Millipore Milli-Q UV system (resistance = 18.2 MΩ·cm). 4(5)-Vinylimidazole and *N*-methyl-4(5)-vinylimidazole were synthesized according to the literature.[15]

2.2. Synthetic procedure

2.2.1. Synthesis of 2-methyl-*N*-methyl-4(5)-vinylimidazole (2M4VIm)

In a dry 200 mL two-necked flask, 2.76 g of *N*-methyl-4(5)-vinylimidazole (25.5 mmol) and 65 mL of dry THF were added. The solution was cooled to -78 °C (dry ice/acetone) under an argon atmosphere. 10.5 mL of *n*-BuLi (2.6 M) was slowly added dropwise, and then stirred at 0 °C for 1 h. Then, 3.97 g of iodomethane (28.0 mmol) was added and stirred at 0 °C for 30 min. Subsequently, the reaction mixture was stirred at room temperature for another 30 min and

then poured into water and extracted four times with dichloromethane. The organic layer was combined together and dried over K_2CO_3 for 15 min. The dichloromethane solution was evaporated, and the residue was distilled under reduced pressure (80 °C, 0.2 mmHg) to give two isomeric 2M4VIm. The 2M4VIm was dried under reduced pressure and was finally obtained as a colorless liquid (2.51 g, 81% yield).

^{1}H NMR (300 MHz, $CDCl_3$): 2-methyl-*N*-methyl-4-vinylimidazole: δ = 6.73 (1H, s), 6.53 (1H, dd, *J* = 17.4, 11.1 Hz), 5.76 (1H, dd, *J* = 17.4, 1.8 Hz), 5.05 (1H, dd, *J* = 11.1, 1.8 Hz), 3,53 (3H, s), 2.37 (3H, s); 2-methyl-*N*-methyl-5-vinylimidazole: δ = 7.06 (1H, s), 6.46 (1H, dd, *J* = 17.4, 11.4 Hz), 5.53 (1H, dd, *J* = 17.4, 1.4 Hz), 5.16 (1H, dd, *J* = 11.4, 1.4 Hz), 3.51 (3H, s), 2.38 (3H, s).

2.2.2. Graft polymerization of 2M4VIm and styrene

ETFE films (5×5 cm^2) were added to a dried Schlenk tube. The ETFE film in a Schlenk tube was irradiated by ^{60}Co γ-rays wtih a total dose of 80 kGy at a dose rate of 5 kGy/h for 16 h under an argon atmosphere. A 50 vol% solution of 2M4VIm and styrene (7:3 volume ratio) in 1,4-dioxane was degassed by argon bubbling for at least 10 min and added to a Schlenk tube under argon atmosphere, and the mixture was heated at 60 °C for 0.33–48 h. Then, the films were removed from the solution, washed several times with 1,4-dioxane, and soaked in ethanol under reflux for 2 h to remove residual monomers and the homopolymers. Finally, the obtained poly(2,3-dimethyl-4-vinylimidazole-co-styrene)-grafted ETFE film (ETFE-g-2M4VIm/St) was dried in a vacuum oven at 80 °C for 24 h. The grafting degree (GD) was calculated as below:

$$GD\ (\%) = \frac{W_g - W_0}{W_0} \times 100 \quad (1)$$

where W_0 and W_g are the weights of the film before and after graft polymerization, respectively.

2.2.3. Quaternization of ETFE-g-2M4VIm/St by *N*-alkylation and ion-exchange reaction

For *N*-alkylation, ETFE-g-2M4VIm/St was immersed in 1 M iodomethane/1,4-dioxane solution at 60 °C for 24 h according to the literature.[12b-12e] The obtained film was washed several times with 1,4-dioxane and soaked in 1 M HCl solution at 60 °C for 3 h. The solution was replaced twice every hour to promote the ion-exchange reaction. The membrane was removed and dried in a vacuum oven at 80 °C for 24 h to obtain poly(1,2,3-trimethyl-4-vinylimidazolium chloride-co-styrene)-grafted ETFE (2M4VIm/St-AEM-Cl). The molar ratio of imidazole and styrene in the graft chain was estimated by the weight of membranes according to the equations (2)–(5) by assuming that *N*-alkylation proceeded in a 100% yield.

$$\text{2M4VIm/Cl (mol)} = \frac{W_{cl} - W_g}{MW\ of\ CH_3Cl} \tag{2}$$

$$\text{St (mol)} = \frac{W_g - \frac{W_g}{\left(1 + \frac{GD}{100}\right)} - \frac{W_{cl} - W_g}{MW\ of\ CH_3Cl} \times MW\ of\ 2M4VIm}{MW\ of\ St} \tag{3}$$

$$\text{molar ratio of St} = \frac{St\ (mol)}{St\ (mol) + \text{2M4VIm/Cl(mol)}} \times 100 \tag{4}$$

$$\text{molar ratio of 2M4Im/Cl} = \frac{\text{2M4VIm}\ (mol)}{St\ (mol) + \text{2M4VIm/Cl(mol)}} \times 100 \tag{5}$$

where W_{Cl} is the weight of membrane after the quaternization and ion-exchange reactions.

Then, the obtained 2M4VIm/St-AEM-Cl was immersed in a 1 M KOH solution at room temperature for 3 h. The solution was replaced twice every hour to complete the ion-exchange reaction from chloride ions to hydroxide ions. Finally, the obtained poly(1,2,3-trimethyl-4-vinylimidazolium hydroxide-co-styrene)-grafted ETFE (2M4VIm/St-AEM (X/Y)), where X

and Y denote the molar ratio of 2M4VIm and styrene, was washed with nitrogen-saturated water to prevent the absorption of CO_2 and used for the measurements of water uptake and ionic-conductivity as soon as possible.

2MNVIm/St-AEM was prepared according to our previous paper.[12e]

2.3. Characterization and Analysis

2.3.1. Characterization

^{1}H nuclear magnetic resonance (NMR) spectra were recorded on Bruker AVANCE 300 spectrometer (300 MHz). Solid-state ^{13}C NMR experiments were performed with Bruker AVANCE 300 spectrometer (75 MHz) by using cross polarization magic angle spinning (CP-MAS) probe. The membranes were crashed under liquid nitrogen using a ball mill and packed in the rotor. Glycine was used as a reference. Fourier transform infrared (FTIR) spectra were recorded on a HORIBA FT-710 spectrometer equipped with an attenuated total reflectance (ATR) unit (Smith Dura Sample IR II). The in-plane resistance of 2M4VIm/St-AEM was measured at 100 kHz using alternating current impedance spectroscopy with an electrode connected to a LCR meter (HIOKI 3522-50 LCR HiTESTER). The conductivity measurements were carried out at room temperature in a beaker under continuous nitrogen-bubbling. The ionic conductivity was calculated according to Equation (6).

$$\sigma\ (\mathrm{mS/cm}) = \frac{l \times 1000}{R \times S} \tag{6}$$

where l is the distance (cm) between two platinum electrodes, S is the cross-sectional area (cm^2) of the membrane obtained from the thickness multiplied by its width, R (kΩ) is the resistance value from the impedance spectroscopy.

Water uptake was determined as follows. 2M4VIm/St-AEM was hydrated in nitrogen-saturated water at room temperature and lightly wiped with Kimwipes to remove excess water from their surface and calculated using Equation (7).

$$\text{Water uptake}\ (\%) = \frac{W_{wet} - W_{dry}}{W_{dry}} \tag{7}$$

where W_{wet} is the weight of 2M4VIm/St-AEM after immersing the membrane in nitrogen-saturated water and W_{dry} is the weight of the dried 2M4VIm/St-AEM calculated from the weights of the corresponding 2M4VIm/St-AEM-Cl.

IECs were determined by back-titration. 2M4VIm/St-AEM was immersed in 10 mL of 0.5 M HCl standard solution at room temperature overnight. The solution was titrated with a 0.1 M NaOH solution using a titrator. The IEC value was calculated according to the Equation (8).

$$\text{IEC}\ (\text{mmol/g}) = \frac{(V_{ref} - V_{mem}) \times C}{m_{dry}} \tag{8}$$

where V_{ref} and V_{mem} are the volumes of NaOH consumed in the titration without and with the 2M4VIm/St-AEM, respectively. C is the concentration of the NaOH solution and m_{dry} is the weight of 2M4VIm/St-AEM calculated from the weights of the corresponding 2M4VIm/St-AEM-Cl.

The mechanical properties were measured using ASTM-D-1288-1 (A&D Co. Ltd., Japan). The 2M4VIm/St-AEM-Cl were cut into the shape of dog bone with the size of 5×1 cm^2. The tensile strength and elongation at break of 2M4VIm/St-AEM-Cl were measured five times at room temperature, and its average value was used.

2.3.2. SANS measurement

SANS measurements were performed on KWS-2 SANS diffractometer operated by Juelich Centre for Neutron Science at the neutron source Heinz Maier-Leibnitz (FRM II reactor) in Garching, Germany.[16] The incident neutron beam at KWS-2 was monochromatized with a velocity selector to have the average wavelength (λ) of 5 Å with a wavelength resolution of $\Delta\lambda/\lambda$ = 20%. The scattering patterns were collected with a two-dimensional scintillation detector and circularly averaged to obtain scattering intensity profiles as a function of q, where q is the scattering vector and defined by $q = (4\pi/\lambda)\sin(\theta/2)$. λ and θ are neutron wavelength and scattering angles, respectively. The obtained scattering profiles were corrected for the instrument background, detector sensitivity, and scattering from empty cell and finally calibrated to absolute scale (cm^{-1}) using a Plexiglas secondary standard. All the measurements were performed at 25 ± 0.5 °C.

3. Results and Discussion

3.1. Preparation of AEM

2M4VIm was synthesized in a three-step process according to a modified procedure from the literature, except for the third step (methylation at the imidazole C2 position) (**Scheme 2**).[15] Urocanic acid was easily converted to 4(5)-vinylimidazole by decarboxylation at 240 °C under reduced pressure. The viscous liquid was obtained with a yield of 41% by vacuum distillation. The obtained viscous liquid was cast on the polyethylene sheet for the crystallization of 4(5)-vinylimidazole. For *N*-methylation, 4(5)-vinylimidazole was reacted with iodomethane in the presence of sodium hydride at a temperature range from 0 °C to room temperature to prevent polymerization as a side reaction. Although *N*-methyl-4(5)-vinylimidazole was purified by a Florisil column in a previous paper,[15b] the crude product was readily purified by vacuum distillation without column chromatography, yielding a colorless liquid (58% yield). The structure of *N*-methyl-4(5)-vinylimidazole consisting of two isomers, 1-methyl-4-vinylimidazole and 1-methyl-5-vinylimidazole with a molar ratio of 3:2, was confirmed using

^{1}H NMR, as reported in the literature.[15b] Then, to introduce the methyl group at the C2 position, *N*-methyl-4(5)-vinylimidazole was lithiated with *n*-BuLi and methylated at the C2 position with iodomethane. The product was obtained by vacuum distillation with a yield of 81%, and the overall yield in three steps was 19%. After introducing the methyl group at the C2 position, the C2 hydrogens of *N*-methyl-4(5)-vinylimidazole at 7.36 and 7.38 ppm disappeared, and new peaks, which were attributed to the methyl groups at the C2 position, were observed at 2.36 and 2.38 ppm in ^{1}H NMR. Any impurity was not observed in ^{1}H NMR and the purity of the obtained 2M4VIm evaluated by ^{1}H NMR was > 98%, which was acceptable for the graft polymerization. It is known that 2M4VIm is easily isolated by vacuum distillation without column chromatography to be obtained in tens of gram quantities. We used a mixture of two isomers of 2M4VIm, 1,2-dimethyl-4-vinylimidazole and 1,2-dimethyl-5-vinylimidazole, because 2M4VIm-grafted membranes have the same structure after polymerization of graft and quaternization of the two isomers.

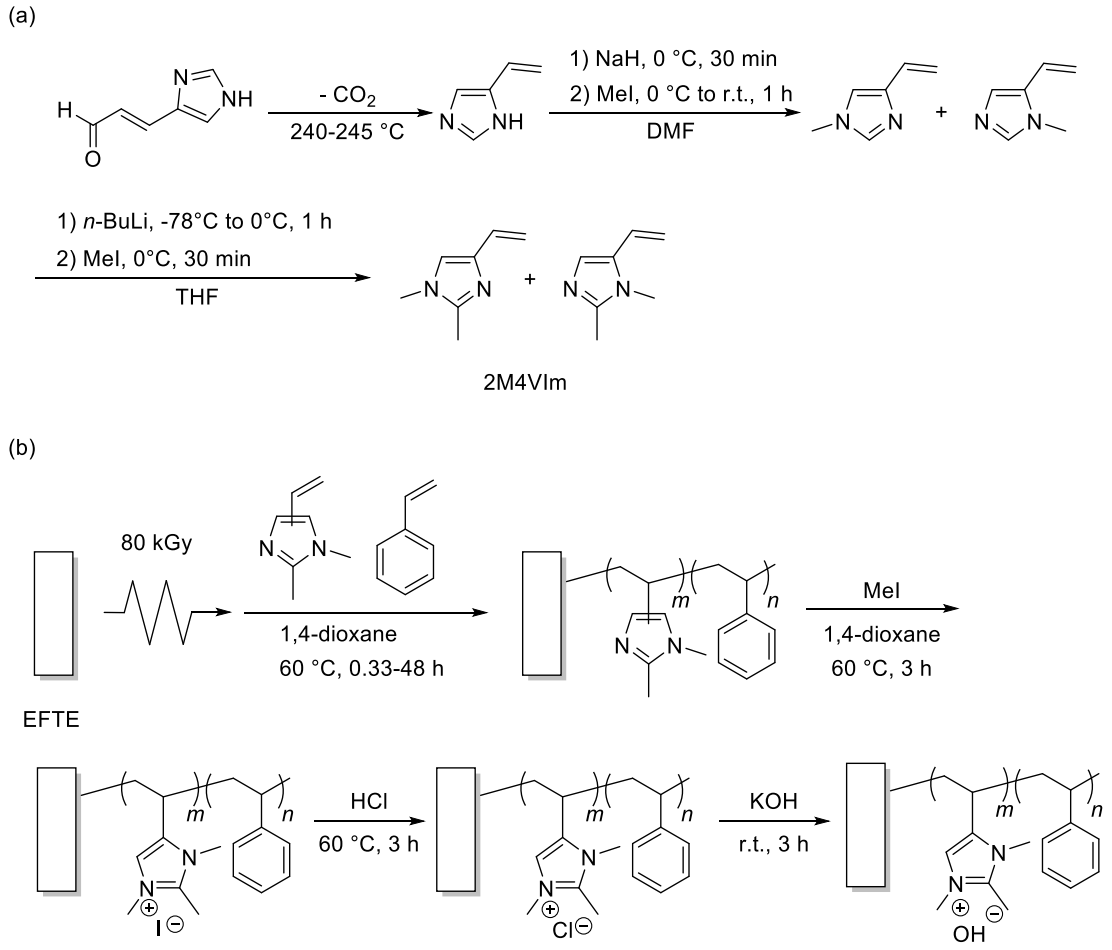

Scheme 2. (a) Synthesis of 2M4VIm. (b) Preparation procedure of AEM. (b) Radiation-induced graft polymerization of 2M4VIm and styrene into a ETFE film, *N*-methylation by iodomethane, and the ion-exchange reaction by HCl and KOH.

The procedure for preparing 2M4VIm/St-AEM is shown in **Scheme 2**. The radiation-induced graft polymerization of 2M4VIm and styrene in the ETFE film was conducted, followed by *N*-alkylation and ion exchange reactions. First, we conducted the graft polymerization of 2M4VIm and styrene by changing the radiation and graft polymerization conditions to control the GD and molar ratio of 2M4VIm and styrene in the graft chain. Recently, we found that the reactivity of 2MNVIm is lower than that of styrene in the radiation-induced graft polymerization in ETFE.[12e] Because of a similar structure of 2M4VIm to that of 2MNVIm, we employed higher volume feed ratios of 2M4VIm/St (7/3) for the graft polymerization to obtain 2M4VIm/St-grafted ETFE having a similar molar ratio of 2M4VIm/St

in the graft chain with a variety GD range. At the beginning of the graft polymerization of 2M4VIm and styrene, the GD rapidly increased and reached 55% in 6 h; thereafter, the GD slowly increased to up to 70% in 48 h. As shown in **Figure 1**, controlling the GDs between 18% and 70% with relatively constant molar ratios of 2M4VIm/St (1/1) in the grafted ETFE was possible by changing the grafting time in the range 0.33–48 h. Since ETFE-g-2M4VIm/St is insoluble in any aqueous and organic solvents, the molar ratio of 2M4VIm and styrene cannot be estimated from the ^{1}H NMR. Therefore, the molar ratios of 2M4VIm and styrene are estimated based on titrimetric and gravimetric methods (vide infra).

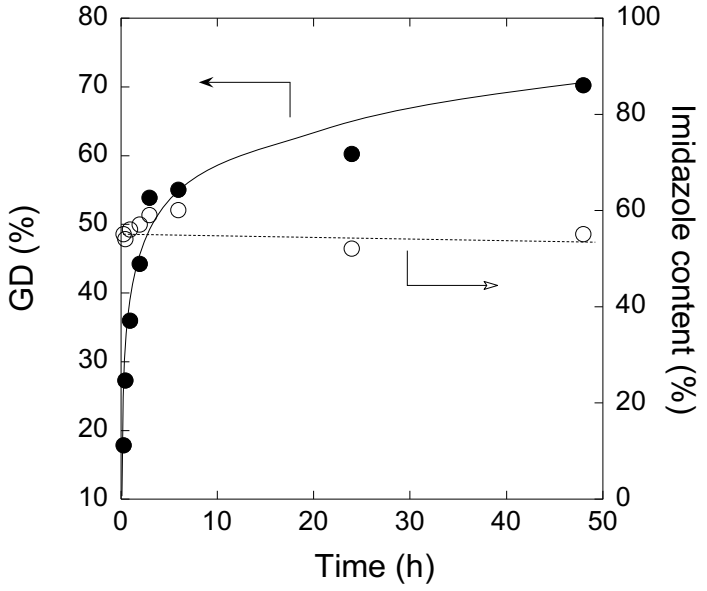

Figure 1. Plots of GD of 2M4VIm and styrene into ETFE films at 60 °C (dark circles) and the imidazole content in the graft chain (light circles).

Next, *N*-alkylation by iodomethane and the ion exchange reaction from the iodide to hydroxide were conducted in a three-step process because the ion exchange reaction from the iodide to hydroxide was too slow, as reported in our previous paper.[12b] The obtained ETFE-g-2M4VIm/St was reacted with iodomethane in 1,4-dioxane at 60 °C according to the literature.[12c–12e] Then, the iodide form of 2M4VIm/St-AEM was converted to the chloride form by soaking in 1 M HCl at 60 °C for 3 h. To confirm the progress of *N*-alkylation and ion

exchange reaction, ETFE-g-2M4VIm/St with GDs 43%–53% and the corresponding 2M4VIm/St-AEM-Cl were prepared. The examples of the solid-state ^{13}C NMR spectra of ETFE-g-2M4VIm/St and the corresponding 2M4VIm/St-AEM-Cl are shown in **Figure 2**. In ETFE-g-2M4VIm/St, the peaks at 25 and 120 ppm were attributed to the polymer chains of ETFE. The peaks attributed to the imidazolium group and styrene unit were overlapped in the range 120–150 ppm. The ethylene group derived from the graft chain was observed at 35 and 43 ppm, respectively. Furthermore, the methyl groups at C2 and C1(C4) positions were observed at 15 and 35 ppm, respectively. Due to the *N*-methylation and ion exchange reactions, a new peak appeared at 39 ppm corresponding to the methyl group at the C1 position. The abovementioned ^{13}C NMR spectral changes were similar to those of the chloride form of 2MNVIm/St-AEM, as reported in a previous article.[12e]

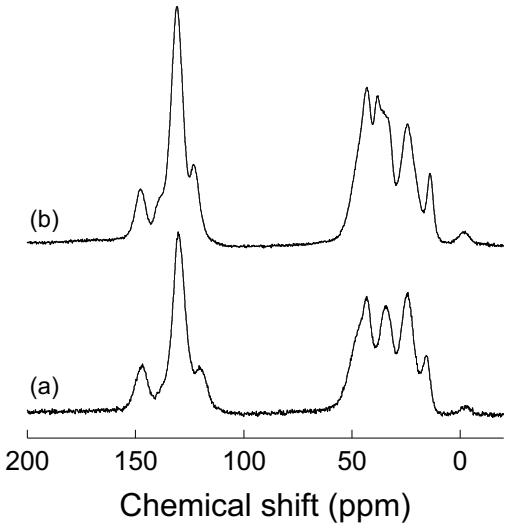

Figure 2. ^{13}C solid-state NMR spectra of (a) ETFE-g-2M4VIm/St and (b) the corresponding 2M4VIm/St-AEM-Cl.

Assuming that *N*-alkylation steadily proceeds until the *N*-methylation degree is 100%, the molar ratios of 2M4VIm and styrene can be estimated using Equations (4) and (5) and are

plotted in **Figure 1**. The molar ratios of 2M4VIm and styrene were roughly 6:4 regardless of the GDs. Additionally, we conducted the graft polymerization of 2M4VIm and styrene to obtain the graft-type AEM, different from the composition of 2M4VIm and styrene in the graft chain. The graft polymerization of 2M4VIm and styrene with feed volume ratios of 9:1, 4:6, and 3:7 gave molar ratios of 75:25, 31:69, and 20:80 for 2M4VIm and styrene units in the graft polymers, respectively (Entries 5–7 in **Table 1**). The composition of 2M4VIm in the graft chain was slightly lower than that in the feed ratio because of the low reactivity of 2M4VIm than that of styrene, as mentioned in the GD results. Indeed, the graft polymerization of 2M4VIm in ETFE needed a high dose of 160 kGy to obtain ETFE-g-2M4VIm with a GD of 48% (Entry 8 in **Table 1**).[12c] Finally, the ion exchange reaction from the chloride to the hydroxide form was conducted in 1 M KOH solution at room temperature for 3 h, and the obtained AEM was washed with nitrogen-saturated water.

Table 1. Conductivity, water uptake, ion exchange, and IEC of 2M4VIm/St-AEM (X/Y)[a]

Entry	2M4VIm/St-AEM (X/Y)	GD (%)	2M4VIm:St	Conductivity[b] (mS/cm)	Water uptake[b] (%)	$IEC_{obs.}$ (mmol/g)	$IEC_{cal.}$ (mmol/g)
1	2M4VIm/St-AEM (6/4)	18	55:45	16	15	0.56	0.72
2	2M4VIm/St-AEM (6/4)	36	56:44	23	24	0.96	1.2
3	2M4VIm/St-AEM (6/4)	44	57:43	49	51	1.3	1.5
4	2M4VIm/St-AEM (6/4)	70	55:45	75	60	1.7	1.9
5	2M4VIm/St-AEM (3/7)	56	31:69	31	29	1.0	0.98
6	2M4VIm/St-AEM (2/8)	113	20:80	38	30	0.99	0.97
7	2M4VIm/St-AEM (8/2)	54	75:25	157[c]	86	1.35	2.05
8	2M4VIm-AEM	48	100:0	226[c]	107	1.74	2.21

[a]X and Y denote the molar ratio of 2M4VIm and styrene
[b]Measured at room temperature.
[c]Measured at 60 °C.

3.2. Property and structures of 2M4VIm/St-AEM (6/4)

3.2.1 Electrolyte properties

The conductivity and water uptake of 2M4VIm/St-AEM (X/Y), where X and Y denote the molar ratio of 2M4VIm and styrene, are listed in **Table 1**. As shown in Entries 1–4,

2M4VIm/St-AEM (6/4) with IECs of 0.56, 0.96, 1.3, and 1.7 mmol/g exhibited conductivities of 16, 23, 49, and 75 mS/cm and water uptakes of 15%, 24%, 51%, and 60%, respectively. Compared with the graft-type AEM with the tetraalkylammonium group (TMA-AEM) with an IEC of 1.56 mmol/g, which showed a conductivity of 111 mS/cm and water uptake of 94%, 2M4VIm/St-AEM (6/4) with an IEC of 1.7 mmol/g showed lower conductivity and water uptake.[12d] On the other hand, the conductivity and water uptake of 2M4VIm/St-AEM (6/4) were similar to those of An-AEM with a similar IEC (1.59 mmol/g), which exhibited 74 mS/cm conductivity and 66% water uptake.[12d] The ionic group of the graft-type AEM greatly affected its conductivity and water uptake.

As we had previously reported, the basicity of 2M4VIm/St-AEM must be lower than that of TMA-AEM because the conjugated imidazolium hydroxide is a weaker base than that of tetraalkylammonium hydroxide.[14] Accordingly, 2M4VIm/St-AEM (6/4) showed lower conductivity and water uptake than those of TMA-AEMs. The relatively moderate electrolyte properties of the 2M4VIm/St-AEM (6/4), such as high conductivity with low water uptake, were attributed to the basicity of the imidazolium group and the hydrophobic styrene in the graft chain, as we previously reported.[12e] On the other hand, the slightly higher conductivity and water uptake of 2M4VIm/St-AEM (6/4) compared with those of 2MNVIm/St-AEM (6/4) (44 mS/cm and 35%) should result from the imidazolium cation in the graft chain rather than the difference in the basicity between 2M4VIm and 2MNVIm.

To understand the spacer effect of styrene in the graft chain on the electrolyte properties, 2M4VIm/St-AEM with similar IECs with different molar ratios of 2M4VIm and styrene (X/Y) were prepared. As shown in Entries 2, 5, and 6 (**Table 1**), 2M4VIm/St-AEMs (6/4), (3/7), and (2/8) exhibited conductivities of 23, 31, and 38 mS/cm and water uptakes of 24%, 29%, and 30%, respectively. The conductivity and water uptake increased when the styrene contents increased from 44% to 80% in the graft chain, although the IECs of 2M4VIm/St-AEMs (6/4), (3/7), and (2/8) were similar. This phenomenon was observed in 2MNVIm/St-AEM, namely, it

may be due to the enlargement of hydrophilic region and the increase in the free volume by introducing styrene group, resulting in better percolation of anionic cations, in a previous paper.[13c]

3.2.2 Alkaline stability

We have reported the alkaline stabilities of Im-AEM, An-AEM, and 2MNVIm/St-AEM in 1 M KOH at 80 °C.[12b–12e,13c] *N*-vinylimidazolium cations were subjected to β-elimination because of very acidic protons at β-carbons from two imidazolium nitrogen atoms (double β-carbon). As mentioned in the introduction, the styrene in the graft polymers improved the alkaline durability of graft-type AEMs even though the random insertion of styrene between 2MNVIm units in the graft polymers did not remove all the double β-carbon from the imidazolium group. To systematically understand the structure–alkaline durability relationship, the alkaline stabilities of 2M4VIm/St-AEM was evaluated in 1 M KOH at 80 °C, which is the expected operating condition of alkaline fuel cell systems, and compared with that of 2MNVIm/St-AEM with a similar monomer ratio and IEC. As shown in **Figure 3** (a), the conductivities of 2MNVIm/St-AEM (6/4) (IEC = 1.6 mmol/g) rapidly decreased at an early stage and to 23% of the initial level in 96 h. Thereafter, they slowly declined and exhibited a conductivity of 11.5 mS/cm even after 600 h. On the other hand, the conductivities of 2M4VIm/St-AEM (6/4) gradually decreased from the initial value (82 mS/cm) with increasing immersion time and reached 3.8 mS/cm after 432 h, as shown in **Figure 3** (a).

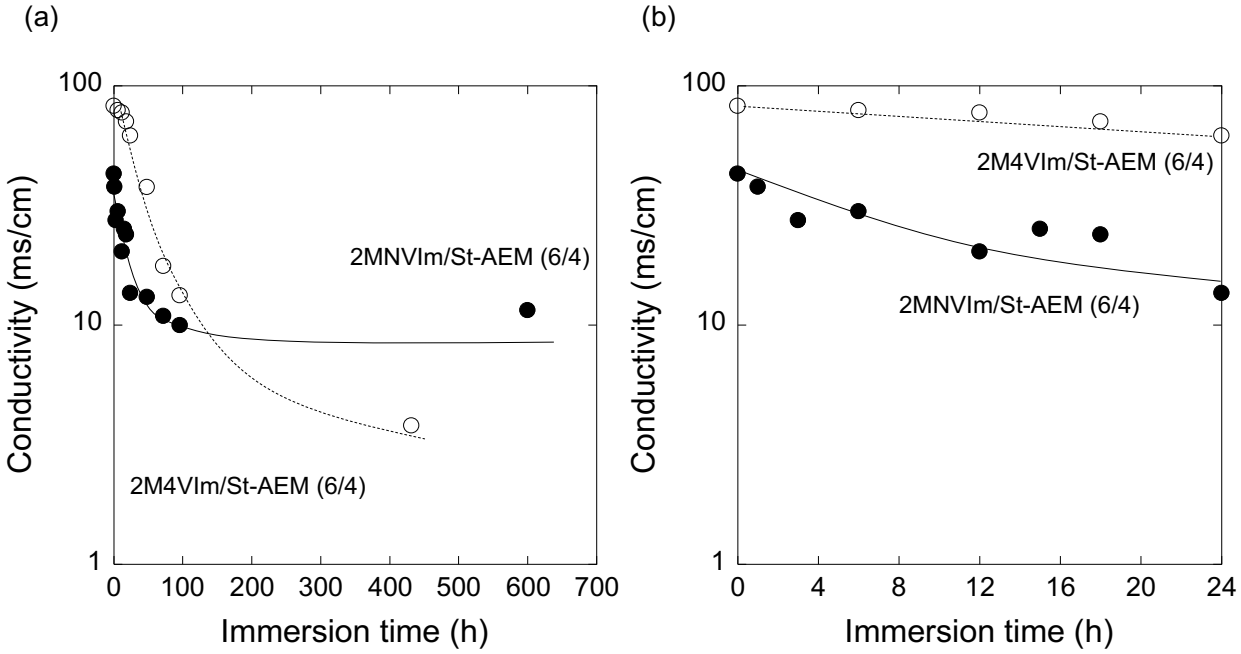

Figure 3. (a) Time course of conductivities of 2M4VIm/St-AEM (6/4) with an IEC of 1.7 mmol/g (light circles) and 2MNVIm/St-AEM (6/4) with an IEC of 1.6 mmol/g (dark circles) after immersion in 1 M KOH at 80 °C, measured at room temperature in nitrogen-saturated deionized water. (b) Magnified time course of conductivities in the range of 0–24 h.

As reported in previous papers, 2MNVIm/St-AEM showed two-step degradation: fast β-elimination and slow hydrolytic ring-opening reactions of the imidazolium ring.[12e,13c] The solid-state ^{13}C NMR of 2MNVIm/St-AEM suggested the detachment of the imidazolium group, but not the ring-opening reaction of the imidazolium group.[12e] 2M4VIm/St-AEM (6/4) slowly decomposed at an initial stage, resulting from the suppression of the β-elimination of the imidazolium group. As shown in **Figure 3** (b), 2M4VIm/St-AEM maintained high conductivities until 24 h; then, the conductivity decreased with increasing immersion time. Thus, the structural design of 2M4VIm, which has no β-protons, suppresses β-elimination at an early stage in the alkaline condition. The successful suppression of the β-elimination of the

imidazolium group was also supported by negligible changes in the IEC of 2M4VIm/St-AEM within 24 h, as shown in **Figure 4** (a).

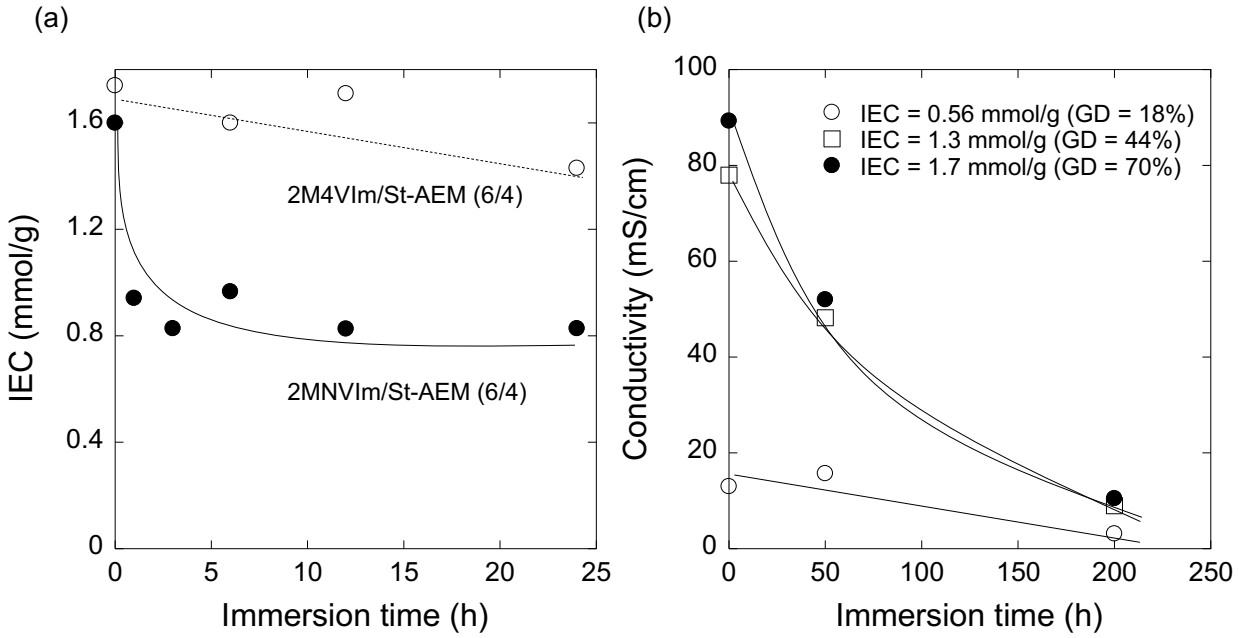

Figure 4. (a) IECs of 2M4VIm/St-AEM (6/4) with an IEC of 1.7 mmol/g (light circles) and 2MNVIm/St-AEM (6/4) with an IEC of 1.6 mmol/g (dark circles) after immersion in 1 M KOH aqueous solution at 80 °C. (b) Changes in the conductivities of 2M4VIm/St-AEM (6/4) with an IEC of 0.56 (light circles), 1.3 (light squares), and 1.7 (dark circles) mmol/g after immersion in 1 M KOH at 80 °C.

The alkaline stability of typical AEMs increases when the hydrophobicity of the polymer matrix increases because the increased hydrophobicity of the polymer matrix prevents the ionic groups from hydrolysis.[13d,17] Thus, we prepared 2M4VIm/St-AEMs (6/4) with lower IECs (0.56 and 1.3 mmol/g) than that we mentioned above (IEC = 1.7 mmol/g) (Entries 1 and 3 in **Table 1**). 2M4VIm/St-AEM (6/4) with IECs of 0.56, 1.3, and 1.7 mmol/g exhibited conductivities of 16, 49, and 75 mS/cm and water uptakes of 15%, 51%, and 60%, respectively. Similarly, the conductivity decreased for the membrane with a lower IEC (1.3 mmol/g) in the alkaline solution (**Figure 4** (b)). More hydrophobic 2M4VIm/St-AEM with a low IEC (0.56

mmol/g) showed insufficient initial conductivity (16 mS/cm) and a similar decline in conductivity. Unfortunately, the distinct improvement of alkaline stability was not observed by changes in the IECs of 2M4VIm/St-AEM (6/4). In the 2M4VIm/St-AEM, the ring-opening reaction slowly occurred for a longer period of degradation even though the imidazolium group was protected at the C2 position by the methyl group.

We reported that graft-type TMA-AEMs had poor mechanical properties and broke into several pieces after a few hours in 1 M KOH at 80 °C.[12d] As discussed in the section of electrolyte properties, the imidazole groups as the ionic group showed lower basicity; therefore, 2M4VIm/St-AEM was expected to improve the mechanical properties after immersion in alkaline solution. The tensile strength and elongation at break of 2M4VIm/St-AEM-Cl, for which we used the chloride form instead of the hydroxide form of AEM to avoid the transformation from hydroxide to bicarbonate forms and quick water absorption, were measured as mentioned in a previous study.[12a] After immersion in 1 M KOH solution at 80 °C for 24 h, the tensile strength and elongation at break of 2M4VIm/St-AEM-Cl (6/4) decreased from 41 to 26 MPa (63% of the initial value) and from 88% to 61%, respectively, while preserving its shape. The improvement in mechanical property in an alkaline solution is similar to those observed in 2MNVIm/St-AEM (6/4) having an IEC of 1.6 mmol/g, whose tensile strength and elongation at break decreased from 41 to 31 MPa and from 82% to 40%, respectively. The alkaline durability tests for the two imidazolium/St-cografted AEMs proved that weaker basicity of the imidazolium hydroxide in the AEMs, compared with the corresponding aliphatic ammonium hydroxide, is essential for the high alkaline durability of membranes.

3.2.3 Degradation mechanism

To confirm the degradation mechanism, the structural changes of 2M4VIm/St-AEM (6/4) in 1 M KOH aqueous solution at 80 °C was investigated using FTIR-ATR (**Figure 5**).

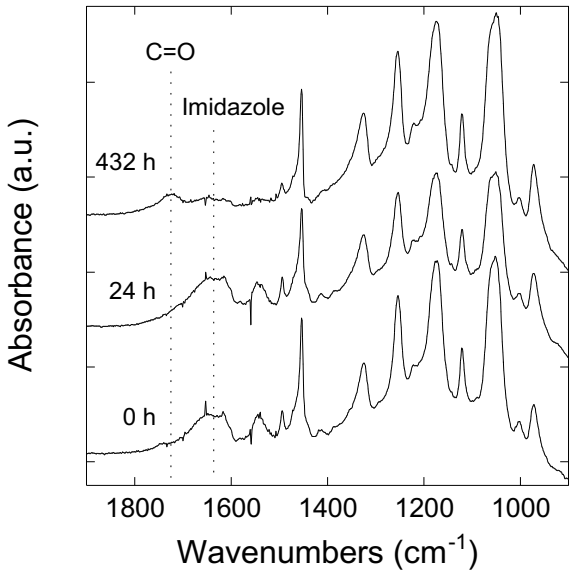

Figure 5. ATR-FTIR spectra of 2M4VIm/St-AEM (Im/St = 6/4) with an IEC of 1.7 mmol/g before and after immersion in 1 M KOH at 80 °C for 432 h.

The peaks attributing to the imidazolium group at 1680 cm^{-1} and ETFE at 1455 cm^{-1} (CH_2) and in the range 1000–1300 cm^{-1} (CF_2) showed no discernible change after immersion in 1 M KOH at 80 °C for 24 h. 2M4VIm/St-AEM maintained the conductivity and IEC in 1 M KOH at 80 °C for 24 h (**Figure 3** (b) and **Figure 4** (a)). However, after 432 h of immersion, the peak of the imidazolium group at 1680 cm^{-1} diminished to 25% of the initial value (estimated from the peak area) with the appearance of a new peak at 1730 cm^{-1} corresponding to the carbonyl group. As shown in **Figure 3** (a), the conductivity of 2M4VIm/St-AEM disappeared after 432 h in 1 M KOH at 80 °C. These spectral and physiochemical changes suggested that 2M4VIm/St-AEM is stable at an early stage in 1 M KOH at 80 °C owing to the suppression of β-elimination of the imidazolium group, and thereafter, the hydroxide anion attacked the carbon at the C2 position of the imidazolium group, resulting in the ring-opening reaction that gives the carbonyl group (**Figure S1**).

In our molecular design, 2M4VIm/St-AEM showed the suppression of β-elimination at an early stage in the alkaline condition.; however, the ring-opening reaction of 2M4VIm/St-AEM

was faster than that of 2MNVIm/St-AEM. Consequently, the conductivity of 2M4VIm/St-AEM became lower than that of 2MNVIm/St-AEM. In the case of 2M4VIm/St-AEM, the C2 position of the imidazolium group, which is attacked by the hydroxide ion, is located outside the graft chain (**Figure S2**). This situation reduces the alkaline durability of the graft-type AEM because the imidazolium ring is not protected by (hydrophobic) styrene, and the hydroxide ion tends to attack the C2 position with no steric hindrance. On the other hand, the imidazolium ring in the 2MNVIm/St-AEM was surrounded by styrene and became more hydrophobic. As mentioned in the section of the electrolyte properties of the graft-type AEMs, 2M4VIm/St-AEM (6/4) exhibited higher conductivities and water uptakes than those of 2MNVIm/St-AEM (6/4) with a similar IEC. The relationship between the alkaline stability and electrolyte properties was consistent with the direction of the C2 position of the imidazolium group, which was an important factor in suppressing the ring-opening reaction of the imidazolium group in 1 M KOH at 80 °C.

3.2.4 Hierarchical structure

To understand the hierarchical structural factors for the electrolyte properties and alkaline durability of the AEMs, we performed SANS measurements on 2M4VIm/St-AEM (6/4) with an IEC of 0.96 mmol/g in a dry state and an equilibrated state in D_2O at room temperature. The intensity profiles, $I(q)$, of the dry and wet states are plotted as a function of scattering vector, q, in **Figure 6**. According to the scattering features at different length scales, the SANS profile was classified into two q-regions: Region I at $q < 0.8$ nm^{-1} was related to the microphase separation of the membrane, whereas Region II at $q > 0.8$ nm^{-1} to the internal structures of ion-conducting channels. In Region I, 2M4VIm/St-AEM (6/4) in D_2O showed a typical correlation peak at $q_1 \sim 0.165$ nm^{-1}, representing a typical lamellar microphase separation structure with an average d spacing ($d_1 = 2\pi/q_1$) of 38 nm. Note that d_1 is larger than that of the AEM in its dry condition because the incorporation of water with graft polymers expanded the

microdomains.[13] At $q > 0.8$ nm^{-1}, $I(q)$ was flat and almost q-independent, indicating no extra nanoscale phase separation at this length scale. The scattering features were the same as those of the previously reported 2MNVIm/St-AEMs (6/4) with distinct conducting and nonconducting two-phase structures. The former phase is composed of a part of graft copolymers (conducting grafts) and water, whereas the latter phase consists of hydrophobic ETFE polymers and the remaining part of the graft polymers (nonconducting grafts).[13b,13c] The similar two-phase structures may result from similar molecular structures in the graft polymers. Thus, we can assume that the hierarchical structure of 2M4VIm/St-AEM (6/4) is very close to those of 2MNVIm/St-AEMs (6/4), which have been systematically investigated in our previous work.[13b,13c] Moreover, for a series of 2MNVIm/St-AEMs (6/4) with the same composition of imidazole and styrene units but different GDs and IECs, we confirmed similar hierarchical structures.[13b] Therefore, we also expect similar structures in 2M4VIm/St-AEMs (6/4) (i.e., Entries 1–4).

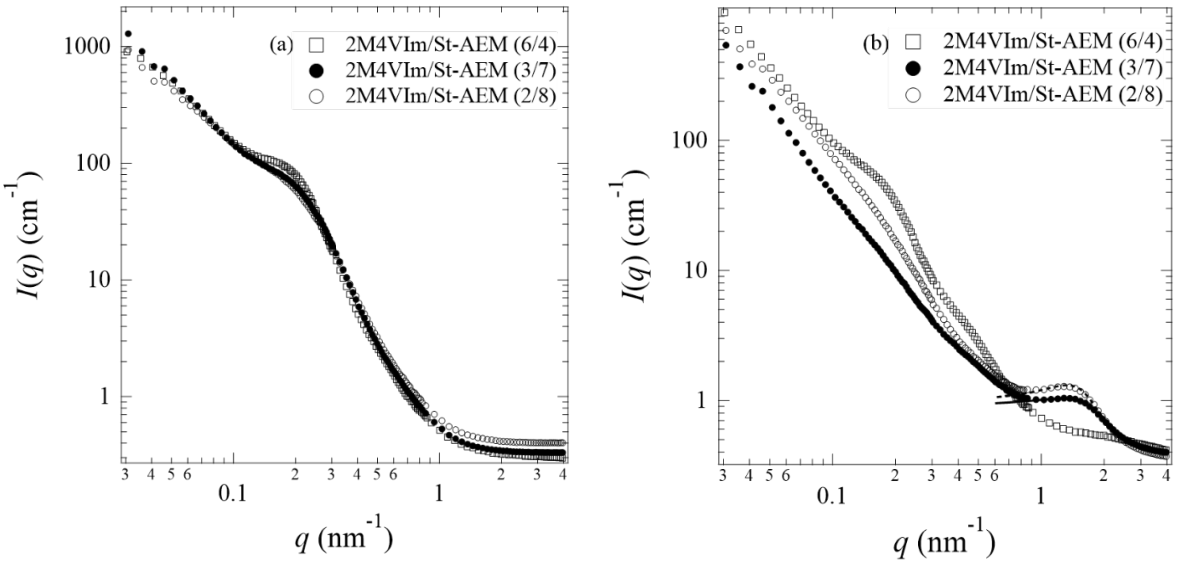

Figure 6. SANS profiles of AEMs having different Im/St ratios measured at room temperature (a) in the dry state; (b) equilibrated in D_2O. The best-fitted theoretical solid and dashed lines were obtained based on the hard-sphere liquid model analysis with the following parameters: the average radius (R_s) and volume fraction (ϕ_S) of spheres are 1.7 nm and 0.17 for 2M4VIm/St-AEM (3/7) and 1.9 nm and 0.205 for 2M4VIm/St-AEM (2/8), respectively.

3.3. Effects of 2M4VIm/St ratios on the properties and structures

The effects of monomer ratios (2M4VIm/St) of the graft polymers on the electrochemical properties and hierarchical structures of the AEMs that have a similar IEC (1.0 mmol/g) were examined by comparing the abovementioned 2M4VIm/St-AEMs (6/4) with more hydrophobic 2M4VIm/St-AEMs (3/7 and 2/8), which had higher hydrophobic styrene contents (Entries 2, 5, and 6 in **Table 1**). The conducting properties and durability in the alkaline solution of these three AEMs are shown in **Table 1** and **Figure 7**. Two hydrophobic 2M4VIm/St-AEMs (2/8 and 3/7) showed slightly higher initial conductivities (31 and 38 mS/cm) and water uptakes (29% and 30%) than those of more hydrophilic 2M4VIm/St-AEMs (6/4) (23 mS/cm and 24%). The larger amounts of graft-polymers in the hydrophobic AEMs should be advantageous to

have larger amounts of water to make better conducting paths, consisted of the graft-polymers and water.

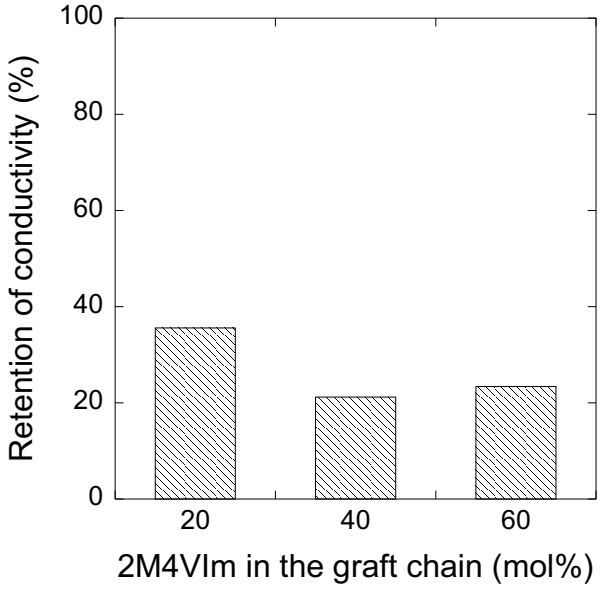

Figure 7. The retention of conductivity of 2M4VIm/St-AEM (6/4) with an IEC of 0.96 mmol/g, 2M4VIm/St-AEM (3/7) with an IEC of 1.0 mmol/g, and 2M4VIm/St-AEM (2/8) with an IEC of 0.99 mmol/g after 200 h in 1 M KOH aqueous solution at 80 °C.

However, these hydrophobic membranes showed similar decremental conductivity profiles as a function of time in the alkaline durability tests compared to that of 2M4VIm/St-AEMs (6/4) even though they possess different hydrophobicity.

For comparison, the SANS profiles of 2M4VIm/St-AEMs (3/7) and (2/8) were also plotted together with 2M4VIm/St-AEMs (6/4) in **Figure 6**. The scattering peak around q_1, corresponding to the *d* spacing of hydrophilic and hydrophobic phases, almost disappeared in 2M4VIm/St-AEM (2/8) and 2M4VIm/St-AEM (3/7) but not in 2M4VIm/St-AEM (6/4) when the D_2O was incorporated in the hydrophilic graft polymer regions. The different behavior due to the imidazolium contents is explained by taking account of the neutron scattering length density (SLD) of the hydrophilic and hydrophobic phases, which can be theoretically calculated

on the basis of the molecular structure and the volume fraction.[13] In AEMs with a dry state, the SLD of the hydrophobic ETFE phase is calculated to be about 2.7 ($\times 10^{10}$ cm^{-2}), which is noticeably larger than that of the dry graft-polymer phase being about 1.33, 1.29 and 1.17 ($\times 10^{10}$ cm^{-2}) for 2M4VIm/St-AEM (2/8) and 2M4VIm/St-AEM (3/7) and 2M4VIm/St-AEM (6/4), respectively. Therefore, it gives a good scattering contrast between ETFE and graft-polymer phases in all dry AEMs, resulting in an obvious peak at q_1. In contrast, for AEMs in D_2O hydrated state, the incorporation of D_2O, which has a much larger SLD value of 6.3×10^{10} cm^{-2}, with the graft-polymer significantly increases the averaged SLD of the hydrophilic phase composed of graft-polymers and D_2O, being about 2.49, 2.43 and 2.17 ($\times 10^{10}$ cm^{-2}) for 2M4VIm/St-AEM (2/8) and 2M4VIm/St-AEM (3/7) and 2M4VIm/St-AEM (6/4), respectively. Thus, the scattering contrast between the hydrophilic and hydrophobic phase in 2M4VIm/St-AEM (2/8) and 2M4VIm/St-AEM (3/7) is much suppressed in comparison with that of 2M4VIm/St-AEM (6/4). Therefore, the peak around q_1 becomes less visible for both 2M4VIm/St-AEM (2/8) and 2M4VIm/St-AEM (3/7) than 2M4VIm/St-AEM (6/4).

Both 2M4VIm/St-AEMs (3/7) and (2/8) showed shoulder-like scattering maxima at approximately q = 1.5 nm^{-1}, which cannot be observed for 2M4VIm/St-AEMs (6/4). The scattering peaks at q ~ 1.5 nm^{-1} originate from the heterogeneous conducting phase separated from the hydrophobic matrix with water puddles, based on the same structure observed in 2MNVIm/St-AEMs with higher hydrophobic styrene contents in the graft polymers (2MNVIm/St ratios = 4/6 and 3/7).[13c] Applying the same analytical method as in the case of 2MNVIm/St-AEMs (a hard-sphere liquid model) to estimate the average radius (R_s) and volume fraction (ϕ_S) of the puddles, we obtained 1.7 nm and 0.17 for 2M4VIm/St-AEM (3/7) and 1.9 nm and 0.205 for 2M4VIm/St-AEM (2/8), respectively.[13c]

As previously reported, hydrophobic 2MNVIm/St-AEMs, which have water puddle structures in the hydrophilic phase, consisted of the graft-polymers with higher St contents, exhibit lower alkaline stability than the corresponding hydrophilic AEMs (lower St

contents).[13c] In contrast, hydrophobic 2M4VIm/St-AEMs with higher St contents (the contents of 2M4VIm are 40% and 20% in Figure 7) showed comparable and even higher alkaline stabilities, respectively, even though they have water puddle structures in hydrophilic phase. One possible reason for the different alkaline stability of the 2MNVIm/St-AEMs and 2M4VIm/St-AEMs AEMs with the water puddle structures should be lower long-term alkaline stability of 2M4VIm/St-AEM than that of 2MNVIm/St-AEM. Namely, 2M4VIm/St-AEM is subject to the ring-opening reaction via the hydroxide attack to the imidazolium group, which orients outward from the hydrophobic graft-polymer chains (Figure S2). These results confirmed the structural transition from a homogeneous to a heterogeneous conducting phase when the hydrophobic St content increases in 2M4VIm/St-AEMs.

4. Conclusion

The β-hydrogen-free imidazole monomer, 2M4VIm, was synthesized using a three-step process with a 19% overall yield. 2M4VIm/St-AEMs (6/4) with IECs of 0.56–1.7 mmol/g were prepared by radiation-induced graft polymerization, *N*-alkylation, and ion exchange reactions. 2M4VIm/St-AEM (6/4) with IECs of 0.56, 0.96, 1.3, and 1.7 mmol/g exhibited conductivities of 16, 23, 49, and 75 mS/cm and water uptakes of 15%, 24%, 51%, and 60%, respectively. The conductivity and water uptake values of 2M4VIm/St-AEMs increased compared with those of previously reported 2MNVIm/St-AEMs with similar comonomer ratios and IECs. The SANS measurements of dry and swollen 2M4VIm/St-AEMs revealed the two-phase hierarchical structures similar to that of 2MNVIm/St-AEM having a similar Im/St composition, comprising hydrophilic layers consisting of partially grafted polymers with water as ion channels. In the alkaline durability test (1 M KOH at 80 °C), 2M4VIm/St-AEMs maintained high conductivities at an early stage in the alkaline condition (for 24 h) because of the suppression of β-elimination. However, the long-term alkaline stability of 2M4VIm/St-AEM was lower than that of 2MNVIm/St-AEM because of the ring-opening reaction via the hydroxide attack to the

imidazolium group, which orients outward from the graft main chain. These findings can provide new insight into imidazolium-based graft-type AEM, namely, the further improvement of steric hindrance of imidazole group will be desired.

Supporting Information
Supporting Information is available from the Wiley Online Library or from the author.

Acknowledgements

This work was partially supported by the Advanced Low Carbon Technology Research and Development Program (ALCA) from the Japan Science and Technology Agency (JST) and Grant-in-Aid for Scientific Research (A) from Japan Society for the Promotion of Science (JSPS) (KAKENHI Grant Number: 18H03850). Shun Watanabe gratefully thanks The Sasakawa Scientific Research Grant in The Japan Science Society (JSS) (Grant number: 27-332). The authors would like to thank Enago for the English Language review.

Received: ((will be filled in by the editorial staff))
Revised: ((will be filled in by the editorial staff))
Published online: ((will be filled in by the editorial staff))

References

[1] R. Borup, J. Meyers, B. Pivovar, Y. S. Kim, R. Mukundan, N. Garland, D. Myers, M. Wilson, F. Garzon, D. Wood, P. Zelenay, K. More, K. Stroh, T. Zawodzinski, J. Boncella, J. E. McGrath, M. Inaba, K. Miyatake, M. Hori, K. Ota, Z. Ogumi, S. Miyata, A. Nishikata, Z. Siroma, Y. Uchimoto, K. Yasuda, K. Kimijima, N. Iwashita, *Chem. Rev.* **2007**, *107*, 3904.

[2] L. Carrette, K. A. Friedrich, U. Stimming, *Fuel Cells* **2001**, *1*, 5.

[3] M. B. Karimi, F. Mohammadi, K. Hooshyari, *Int. J. Hydrogen Energy* **2019**, *44*, 28919.

[4] a) G. Merle, M. Wessling, K. Nijmeijer, *J. Membr. Sci.* **2011**, *1*, 377; b) M. A. Hickner, A. M. Herring, E. B. Coughlin, *J. Polym. Sci., Part B: Polym. Phys.* **2013**, *51*, 1727; c) C. G. Arges, L. Zhang, *ACS Appl. Energy Mater.* **2018**, *1*, 2991.

[5] S. Gottesfeld, D. R. Dekel, M. Page, C. Bae, Y. Yan, P. Zelenay, Y. S. Kim, *J. Power Sources* **2018**, *375*, 170.

[6] a) J. Wang, Z. Zhao, F. Gong, S. Li, S. Zhang, *Macromolecules* **2009**, *42*, 8711; b) M. Tanaka, K. Fukasawa, E. Nishino, S. Yamaguchi, K. Yamada, H. Tanaka, B. Bae, K. Miyatake, M. Watanabe, *J. Am. Chem. Soc.* **2011**, *133*, 10646; c) M. Tanaka, M. Koike, K. Miyatake, M. Watanabe, *Polym. Chem.* **2011**, *2*, 99; d) Z. Zhao, J. Wang, S. Li, S. Zhang, *J. Power Sources* **2011**, *196*, 4445.

[7] a) N. Li, T. Yan, Z. Li, T. T.-Albrecht, W. H. Binder, *Energy Environ. Sci.* **2012**, *5*, 7888; b) N. Li, Y. Leng, M. A. Hickner, C.-Y. Wang, *J. Am. Chem. Soc.* **2013**, *135*, 10124.

[8] a) J. Han, H. Peng, J. Pan, L. Wei, G. Li, C. Chen, L. Xiao, J. Lu, L. Zhuang, *ACS Appl. Mater. Interfaces* **2013**, *5*, 13405; b) X. Wu, W. Chen, X. Yan, G. He, J. Wang, Y. Zhang, X. Zhu, *J. Mater. Chem. A* **2014**, *2*, 12222.

[9] a) Y. Li, A. C. Jackson, F. L. Beyer, D. M. Knauss, *Macromolecules* **2014**, *47*, 6757; b) A. D. Mohanty, C. Y. Ryu, Y. S. Kim, C. Bae, *Macromolecules* **2015**, *48*, 7085; c) K. M. Meek, J. R. Nykaza, Y. A. Elabd, *Macromolecules* **2016**, *49*, 3382.

[10] a) B. Qiu, B. Lin, Z. Si, L. Qiu, F. Chu, J. Zhao, F. Yan, *J. Power Sources* **2012**, *217*, 329; b) Y. Yang, J. Wang, J. Zheng, S. Li, S. Zhang, *J. Membr. Sci.* **2014**, *467*, 48; c) Y. Z. Zhuo, A. L. Lai, Q. G. Zhang, A. M. Zhu, M. L. Ye, Q. L. Liu, *J. Mater. Chem. A* **2015**, *3*, 18105.

[11] a) O. I. Deavin, S. Murphy, A. L. Ong, S. D. Poynton, R. Zeng, H. Herman, J. R. Varcoe, *Energy Environ. Sci.* **2012**, *5*, 8584; b) B.-S. Ko, J.-Y. Sohn, J. Shin, *Polymer* **2012**, *53*, 4652; c) O. M. M. Page, S. D. Poynton, S. Murphy, A. L. Ong, D. M. Hillman, C. A. Hancock, M. G. Hale, D. C. Apperley, J. R. Varcoe, *RSC Advances* **2013**, *3*, 579; d) T. P. Pandey, A. M. Maes, H. N. Sarode, B. D. Peters, S. Lavina, K. Vezzù, Y. Yang, S. D. Poynton, J. R. Varcoe, S. Seifert, M. W. Liberatore, V. D. Noto, A. M. Herring, *Phys. Chem. Chem. Phys.* **2015**, *17*, 4367; e) J. P.-González, D. K. Whelligan, L. Wang, R. B.-Soualhi, Y. Wang, Y. Peng, H. Peng, D. C.

Apperley, H. N. Sarode, T. P. Pandey, A. G. Divekar, S. Seifert, A. M. Herring, *Energy Environ. Sci.* **2016**, *9*, 3724; f) J. P.-González, I. Ouachan, J. R. Varcoe, D. K. Whelligan, *J. Mater. Chem. A* **2018**, *6*, 823; g) A. L. G. Biancolli, D. Herranz, L. Wang, G. Stehlíková, R. B.-Soualhi, J. P.-González, P. Ocón, E. A. Ticianelli, D. K. Whelligan, J. R. Varcoe, E. I. Santiago, *J. Mater. Chem. A* **2018**, *6*, 24330; h) L. Wang, X. Peng, W. E. Mustain, J. R. Varcoe, *Energy Environ. Sci.* **2019**, *12*, 1575.

[12] a) H. Koshikawa, K. Yoshimura, W. Sinnananchi, T. Yamaki, M. Asano, K. Yamamoto, S. Yamaguchi, H. Tanaka, Y. Maekawa, *Macromol. Chem. Phys.* **2013**, *214*, 1756; b) K. Yoshimura, H. Koshikawa, T. Yamaki, H. Shishitani, K. Yamamoto, S. Yamaguchi, H. Tanaka, Y. Maekawa, *J. Electrochem. Soc.* **2014**, *161*, F889; c) Y. Maekawa, K. Yoshimura, K. Takeuchi, A. Hiroki, S. Watanabe, T. Hagiwara, H. Shishitani, S. Yamaguchi, H. Tanaka, *ECS Trans* **2017**, *80*, 979; d) T. Hamada, K. Yoshimura, A. Hiroki, Y. Maekawa, *J. Appl. Polym. Sci.* **2018**, *135*, 46886; e) K. Yoshimura, A. Hiroki, H.-C. Yu, Y. Zhao, H. Shishitani, S. Yamaguchi, H. Tanaka, Y. Maekawa, *J. Membr. Sci.* **2019**, *573*, 403.

[13] a) Y. Zhao, K. Yoshimura, H. Shishitani, S. Yamaguchi, H. Tanaka, S. Koizumi, N. Szekely, A. Radulescu, D. Richter, Y. Maekawa, *Soft Matter* **2016**, *12*, 1567; b) K. Yoshimura, Y. Zhao, S. Hasegawa, A. Hiroki, Y. Kishiyama, H. Shishitani, S. Yamaguchi, H. Tanaka, S. Koizumi, M.-S. Appavou, A. Radulescu, D. Richter, Y. Maekawa, *Soft Matter* **2017**, *13*, 8463; c) K. Yoshimura, Y. Zhao, A. Hiroki, Y. Kishiyama, H. Shishitani, S. Yamaguchi, H. Tanaka, S. Koizumi, J. E. Houston, A. Radulescu, M.-S. Appavou, D. Richter, Y. Maekawa, *Soft Matter* **2018**, *14*, 9118; d) Y. Zhao, K. Yoshimura, H.-C. Yu, Y. Maekawa, A. Hiroki, Y. Kishiyama, H. Shishitani, S. Yamaguchi, H. Tanaka, S. Koizumi, M.-S. Appavou, J. Houston, A. Radulescu, D. Richter, *Physica B: Condens. Matter* **2018**, *551*, 203; e) Y. Zhao, K. Yoshimura, H. Takamatsu, A. Hiroki, Y. Kishiyama, H. Shishitani, S. Yamaguchi, H. Tanaka, S. Koizumi, A. Radulescu, M.-S. Appavou, Y. Maekawa, *J. Electrochem. Soc.* **2019**, *166*, F472; f) Y. Zhao, K. Yoshimura, A. M. A. Mahmoud, H.-C. Yu, S. Okushima, A. Hiroki, Y. Kishiyama, H.

Shishitani, S. Yamaguchi, H. Tanaka, Y. Noda, S. Koizumi, A. Radulescu, Y. Maekawa, *Soft Matter* **2020**, *16*, 8128.

[14] B.-S. Ko, K. Yoshimura, S. Warapon, H. Shishitani, S. Yamaguchi, H. Tanaka, Y. Maekawa, *J. Polym. Sci., Part A: Polym. Chem.* **2019**, *57*, 503.

[15] a) C. G. Overberger, N. Vorchheimer, *J. Am. Chem. Soc.* **1963**, *85*, 951; b) C. G. Overberger, T. W. Smith, *Macromolecules* **1975**, *8*, 401; c) C. G. Overberger, Y. Kawakami, *J. Polym. Sci.: Polym. Chem. Ed.* **1978**, *16*, 1237; d) M. H. Allen, Jr., S. T. Hemp, A. E. Smith, T. E. Long, *Macromolecules* **2012**, *45*, 3669.

[16] A. Radulescu, V. Pipich, H. Frielinghaus, M. S. Appavou, *J. Phys.: Conf. Ser.* **2012**, *351*, 012026.

[17] a) A. D. Mohanty, C. Bae, *J. Mater. Chem. A* **2014**, *2*, 17314; b) H.-S. Dang, E. A. Weiber, P. Jannasch, *J. Mater. Chem. A* **2015**, *3*, 5280; c) H.-S. Dang, P. Jannasch, *Macromolecules* **2015**, *48*, 5742; d) M. G. Marino, K. D. Kreuer, *ChemSusChem* **2015**, *8*, 513.